Article

Interface Bonding Properties of CrAlSiN-Coated Cemented Carbides Doped with CeO_2 and Y_2O_3 Rare Earth Oxides

Junru Yang [1], Yanping Yue [1], Yan Wang [2] and Yuekan Zhang [1,*]

[1] College of Mechanical and Electronic Engineering, Shandong University of Science and Technology, Qingdao 266590, China; yangjunru@sdust.edu.cn (J.Y.); yue171442@163.com (Y.Y.)
[2] Sinopec Qilu Company Ltd., Zibo 255400, China; 19862267401@163.com
[*] Correspondence: zhangyk2007@sdust.edu.cn

Abstract: This study performed first-principle-based calculations of the interface adhesion work in interface models of three terminal systems: $CrAlSiN_{Si}$/WC-Co, $CrAlSiN_{N}$/WC-Co, and $CrAlSiN_{Al}$/WC-Co. The results proved that the $CrAlSiN_{Si}$/WC-Co and $CrAlSiN_{Al}$/WC-Co interface models had the highest and lowest interface adhesion work values (4.312 and 2.536 J·m^{-2}), respectively. Thus, the latter model had the weakest interface bonding property. On this basis, rare earth oxides CeO_2 and Y_2O_3 were doped into the Al terminal model ($CrAlSiN_{Al}$/WC-Co). Then, doping models of CeO_2 and Y_2O_3 doped on the WC/WC, WC/Co, and $CrAlSiN_{Al}$/WC-Co interfaces were established. The adhesion work value was calculated for the interfaces in each doping model. When CeO_2 and Y_2O_3 were doped in the WC/WC and $CrAlSiN_{Al}$/WC-Co interfaces, four doping models were constructed, each model contains interfaces withreduced adhesion work values, indicating deteriorated interface bonding properties. When the WC/Co interface was doped with CeO_2 and Y_2O_3, the interface adhesion work values of the two doping models are both increased, and Y_2O_3 doping improved the bonding properties of the Al terminal model ($CrAlSiN_{Al}$/WC-Co) more significantly than CeO_2 doping. Next, the charge density difference and the average Mulliken bond population were estimated. The WC/WC and $CrAlSiN_{Al}$/WC-Co interfaces doped with CeO_2 or Y_2O_3, with decreased adhesion work, exhibited low electron cloud superposition and reduced values of charge transfer, average bond population, and interatomic interaction. When the WC/Co interface was doped with CeO_2 or Y_2O_3, superposition of the atomic charge densities of electron clouds was consistently observed at the $CrAlSiN_{Al}$/WC-Co interface in the $CrAlSiN_{Al}$/WC/CeO_2/Co and $CrAlSiN_{Al}$/WC/Y_2O_3/Co models; the atomic interactions were strong, and the interface bonding strength increased. When the WC/Co interface was doped with Y_2O_3, the superposition of atomic charge densities and the atomic interactions were stronger than for CeO_2 doping. In addition, the average Mulliken bond population and the atomic stability were also higher, and the doping effect was better.

Keywords: rare earth oxides; CrAlSiN/WC-Co cemented carbide; adhesion work; charge density difference; average Mulliken bond population

1. Introduction

CrAlSiN-coated cemented carbide tools are widely known for their high hardness, corrosion resistance, wear resistance, and high-temperature oxidation resistance. These features have made them especially suitable for machining difficult-to-process materials, such as titanium alloys [1–4]. However, CrAlSiN-coated cemented carbide tools are more commonly associated with interface problems, such as coating disbondment and sticking [5]. Some scholars have doped additives into the coating or matrix to improve the interface properties of the coated cutting tools. For example, Lu et al. [6] prepared a diamond coating with a level of 8000 ppm doped B on the WC-Co cemented carbide matrix and found that, compared with undoped coated cutting tools, the residual stress was lower and the coating–matrix bonding strength was higher. Wang et al. [7] prepared a CrBN

coating containing Ni or Cu doping on a 45 steel matrix. It was found that the coating hardness decreased after adding Ni or Cu, but the coating resistance to circular cracks was significantly enhanced due to good bonding properties between coating substrates. Yu et al. [8] utilized a cathodic arc evaporation system to prepare AlTiN coatings with various B/C doping ratios. The indentation method was used to evaluate the bonding strength between the coating and substrate. The results showed that the bonding strength between the coating and substrate was the best when the B/C ratio was 1:1.

Rare earth elements have high chemical activity and low electronegativity [9,10]. Extensive studies have been conducted worldwide on the reinforcement of material performance using rare earth element doping, which has been found to improve the interface bonding strength. Li et al. [11] employed the sol–gel method to prepare WC-10 (Co, x-Re) composite powders with various rhenium content levels. Microstructural analysis showed that adding rhenium resulted in a more regular WC grain shape and more equiaxed grains. In addition, the interface between the Co binder phase and WC was smooth and without pores, and the interface bonding was satisfactory. Liu et al. [12] reported that doping rare earth elements into WC-Co cemented carbides inhibited grain growth, refining the grains and increasing the interface bonding strength. Zou et al. [13] proved that doping with appropriate amounts of rare earth borides LaB_6 and CeB_6 purified the grain and phase boundaries and improved the WC/Co interface wettability, thereby increasing the interface bonding strength. Wang et al. [14] manufactured WC-11Co cemented carbides with and without CeO_2 doping by vacuum hot-pressing sintering. Their study showed that CeO_2 addition significantly improved the cutter's fracture toughness. Wen [15] doped nano-CeO_2 into WC-10Co cemented carbide and reported that CeO_2 addition improved the fracture toughness of the cemented carbide. The reason was that CeO_2 was enriched at the WC grain boundaries and reacted with impurity elements to purify the grain and phase boundaries. As a result, the wettability and bonding strength of the WC/Co interface were improved, finally increasing the grain and phase boundaries' strength and the cemented carbide's fracture toughness. Guo et al. [16] prepared a WC-6Co cemented carbide doped with Y_2O_3. During solid-phase sintering, the doped Y_2O_3 effectively inhibited the growth of WC grains, while Y_2O_3 located in the WC/Co grain boundary separated WC and Co, thereby inhibiting the dissolution and reprecipitation of WC and increasing the interface bonding strength. Wang et al. [17] doped Y_2O_3 into the WC-10Co cemented carbide. They found that the Y_2O_3 particles were pinned to the WC grain and phase boundaries, hindering the diffusion, dissolution, and growth of WC particles and hence refining the grains. Huang [18] used a wet grinding style to study the effects of CeO_2 and Y_2O_3 doping on WC-10Co cemented carbides. The results showed that CeO_2 and Y_2O_3 doping increased the fracture toughness of the cemented carbides from 12.8 $MPa \cdot m^{1/2}$ before doping to 16.7 $MPa \cdot m^{1/2}$ after doping. Yang et al. [19] employed spark plasma sintering (SPS) technology to prepare a WC-8Co-Y_2O_3 cemented carbide. It was found that Y_2O_3 addition increased the WC/Co interface strength, thereby improving the hardness and fracture toughness of the cemented carbide. Qin et al. [20] employed solid–liquid doping and SPS technology to prepare a Y_2O_3-doped WC-12Co cemented carbide. The results showed that the semicoherent interphase boundary between Y_2O_3 and WC increased the hardness and fracture toughness of the Y_2O_3-doped cemented carbide by 2.1 and 9.2%, respectively, compared with that before doping. Deng et al. [21] employed the in situ synthesis and spray drying process to prepare a CeO_2-doped WC-10Co cemented carbide. Their study showed that CeO_2 doping decreased the surface energy differences between the crystal planes while increasing the wettability of the interface between the Co binder phase and WC grains. For this reason, the degree of densification, hardness, and toughness of the cemented carbide were improved.

The above brief survey of existing studies in the relevant field reveals that most of them have focused on the performance of WC-Co cemented carbides doped with rare earth oxides and achieved this purpose experimentally. However, few studies have been conducted on the interface performance of CrAlSiN-coated cemented carbides. From an

atomic perspective, there still needs to be more investigations into the interface bonding mechanism of CrAlSiN-coated cemented carbides doped with rare element oxides. Therefore, in this paper, based on the first-principles method, from the microscopic atomic point of view, the present study focused on the bonding performance of the coating–matrix interface in the interface models of CrAlSiN-coated WC-Co cemented carbides with different terminal atoms. First, we determined the interface model with the worst interface bonding performance. CeO_2 and Y_2O_3 were doped into the WC/WC, WC/Co, and CrAlSiN$_{Al}$/WC-Co interfaces of CrAlSiN-coated cemented carbides. The adhesion work was calculated for each interface model, and the charge density difference and average Mulliken bond population were estimated. On this basis, the influence pattern and the nature of the interface bonding performance of CrAlSiN-coated cemented carbides doped with rare earth oxides were revealed. These research findings are instrumental in the design optimization, popularization, and application of coated cemented carbide cutting tools with improved interface bonding properties.

2. Parameter Selection for Simulation Analysis and Parameter Calculation of Interface Bonding Properties

2.1. Parameter Selection for Simulation Analysis

The main research in this paper was carried out in the CASTEP module of the Materials Studio software. Geometric optimization was implemented for all models (primal cells such as WC, Co, CrN, Al, Si, CeO_2, and Y_2O_3 and all models before and after doping) based on the first principle and density functional theory. The simulation parameters were chosen as follows.

Based on the Monkhorst–Pack algorithm, the k-point grid was set to $5{\times}5{\times}1$. The energy of each unit cell was determined under different cutoff energies, and it was found that the energy of the unit cell tended to converge at the cutoff energy of 400 eV; therefore, Ecut was set to 400 eV. The structure of the original cell was optimized under different exchange correlation functions; we found that when the exchange association function is GGA-PBE, the calculated lattice constants of the optimized cell have the least deviation from the experimental values; therefore, GGA-PBE was selected as the exchange association function. Ultrasoft pseudopotential was chosen to describe the interactions between valence electrons and the nuclei of ions.

The Broyden–Fletcher–Goldfarb–Shanno (BFGS) algorithm was used to optimize the model. The optimization parameters were as follows: the SCF convergence threshold was specified as 1.0×10^{-5} eV/atom; the maximum interatomic interaction was 0.03 eV/Å; the maximum intracrystalline stress was 0.05 GPa; the maximum atomic displacement was 0.001 Å; and the number of iteration steps was 100 [22].

2.2. Parameter Calculation of Interface Bonding Properties

After the geometric optimization of the interface models, simulation calculation was conducted again using the above parameters to obtain the energy on surfaces α and β and the total energy and area of the α/β interface involved in the optimized interface models. Finally, the adhesion work at the interface was estimated using the relevant formula. Adhesion work is an important parameter characterizing interface bonding properties. It is defined as the reversible work required to separate two phases from each other. The higher the adhesion work, the stronger the interatomic bonding at the interface; hence, the stronger the interface bonding properties and the more stable the interface structure. The adhesion work at the interface between α and β can be calculated as follows [23]:

$$W_{ad} = \frac{E_\alpha + E_\beta - E_{\alpha/\beta}}{A} \tag{1}$$

where W_{ad} is the adhesion work, J/m^2; E_α and E_β are the energies of surfaces α and β, eV; $E_{\alpha/\beta}$ is the total energy of the α/β interface system, eV; and A is the area of the interface, Å^2.

3. Analysis of Interface Bonding Properties of the CrAlSiN/WC-Co Model Non-Doped with CeO$_2$ or Y$_2$O$_3$

3.1. Construction of the CrAlSiN/WC-Co Model

3.1.1. Construction of the WC-Co Cemented Carbide Matrix Model

The WC(0001) crystal face with a W terminal atom is the most stable, and Co can replace the C atom on the WC(0001) surface [24,25]. Considering this, we used the Co atoms to replace the C atoms on the WC(0001) surface with W terminal atoms and added a 20 Å vacuum layer to build the WC-Co model with Co content of 10.4 wt%. As shown in Figure 1, this model was used to approximately represent the cemented carbide matrix YG10.
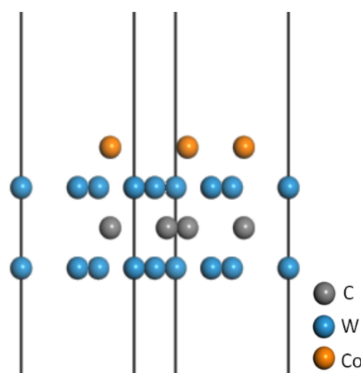

Figure 1. WC-Co model with a vacuum layer.

3.1.2. Construction of the CrAlSiN Coating Model

CrAlSiN and CrAlN grew preferably in the (111) orientation [26]. Al replaced some Cr atoms to become the solid solution in CrN. Si entered the CrAlSiN coating by replacing the Al atoms [27,28]. In addition, the hardness values of the CrAlN and CrAlSiN coatings were higher when Al and Si atoms accounted for 31 and 4.88 wt%, respectively [29,30]. Then, the CrAlN(111) model with Al content of 33 wt%. was built by replacing the Cr atoms in the supercell CrN(111) with Al atoms. Next, Si atoms were used to replace the Al atoms in CrAlN(111), and a 20 Å vacuum layer was added to obtain a CrAlSiN model with Si content of 4.9 wt%. Figure 2 shows a CrAlSiN$_{Al}$ coating model with a vacuum layer.
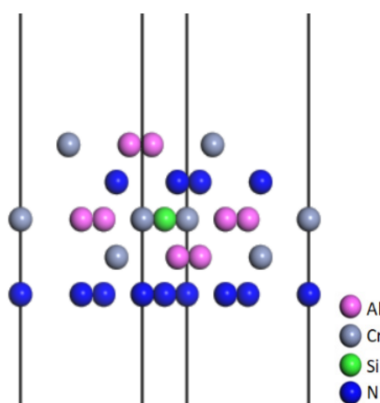

Figure 2. CrAlSiN model with a vacuum layer.

3.1.3. Construction of the CrAlSiN/WC-Co Models with Different Terminal Atoms

The interface bonding strength between the WC-Co matrix and the CrAlSiN coating directly impacted the usability of CrAlSiN-coated cemented carbides. There are three terminal atoms on the CrAlSiN crystal surface: Si, N, and Al. Next, interface models with different terminal atoms were built using the WC-Co cemented carbide matrix and the CrAlSiN coating. The parameters selected for simulation analysis as above were used for

the geometric optimization of the interface models Figure 3 shows the CrAlSiN/WC-Co models with Si, N, and Al terminal atoms after geometric optimization.
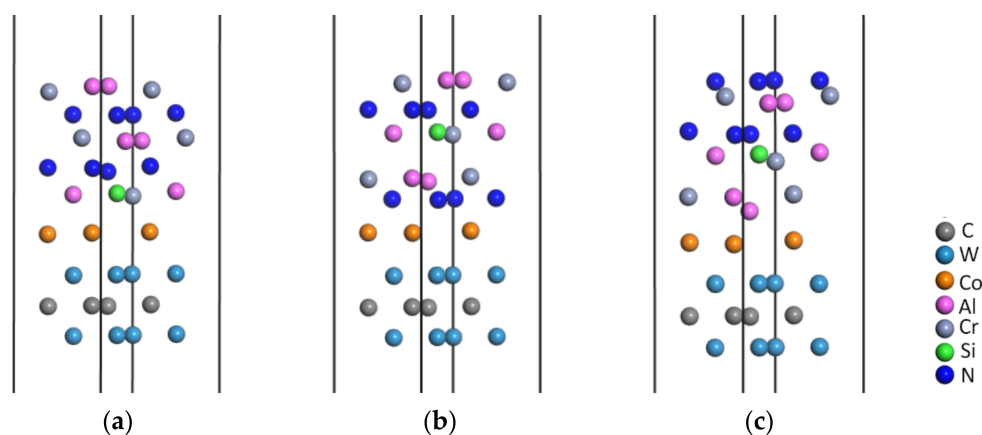

(**a**)   (**b**)   (**c**)

Figure 3. CrAlSiN/WC-Co model after geometric optimization: (**a**) CrAlSiN$_{Si}$/WC-Co; (**b**) CrAlSiN$_N$/WC-Co; (**c**) CrAlSiN$_{Al}$/WC-Co.

3.2. Interface Bonding Property Analysis

Based on the abovementioned parameters, the CrAlSiN/WC-Co models with three different terminal atoms after geometric optimization were used to calculate the total energy $E_{\alpha/\beta}$ on the two surfaces E_α and E_β and the area of the interface $A_{\alpha/\beta}$. The calculated results were substituted into Formula (1) to obtain the adhesion work at the interfaces, as shown in Table 1.

Table 1. Adhesion work of the CrAlSiN/WC-Co model.

Model	E_α/eV	E_β/eV	$E_{\alpha/\beta}$/eV	$A_{\alpha/\beta}$/Å^2	W_{ad}/J·m^{-2}
CrAlSiN$_{Si}$/WC-Co	14,954.098	19,210.462	−34,172.070	27.868	4.312
CrAlSiN$_N$/WC-Co	14,950.463	19,210.372	−34,167.178	27.411	3.702
CrAlSiN$_{Al}$/WC-Co	14,953.219	19,209.751	−34,167.157	26.418	2.536

Table 1 shows that the adhesion work was the largest for the CrAlSiN$_{Si}$/WC-Co model, with a value of 4.312 J·m^{-2}. This model had the highest interface bonding strength and the most stable interface. The adhesion work was the smallest for the Al terminal model (CrAlSiN$_{Al}$/WC-Co), with a value of 2.536 J·m^{-2}. This model had the lowest interface bonding strength and the most unstable interface.

The Al terminal model (CrAlSiN$_{Al}$/WC-Co), the most unstable model, was doped with rare earth oxides CeO$_2$ and Y$_2$O$_3$ to build doped models. The adhesion work at this interface was calculated. The charge density difference and the average Mulliken bond population were analyzed. On this basis, we discussed the effects of doping rare earth oxides on the interface bonding properties of CrAlSiN-coated cemented carbides from the perspectives of charge transfer and bonding mode.

4. Analysis of the Interfaces Bonding Properties of the Al Terminal Model Doped with CeO$_2$ or Y$_2$O$_3$

4.1. Construction of Doped Models

4.1.1. Construction of the CeO$_2$ and Y$_2$O$_3$ Models

The CeO$_2$(001) and Y$_2$O$_3$(001) crystal faces were the most stable. Considering the effects of atoms in the first two layers near the interface on the interface [31], we built the CeO$_2$(001) and Y$_2$O$_3$(001) models with two layers and a 20 Å vacuum layer, A and B are used to show the direction of vacuum layer, as shown in Figure 4.

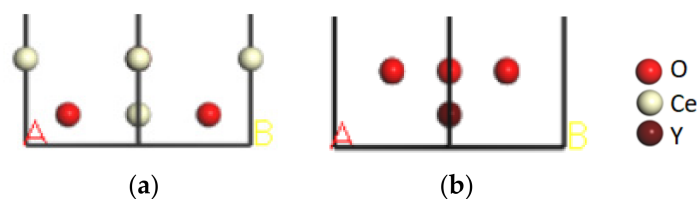**Figure 4.** Rare earth oxide models with a vacuum layer: (**a**) $CeO_2(001)$; (**b**) $Y_2O_3(001)$.

4.1.2. Construction of Al Terminal Models Doped with CeO_2 or Y_2O_3

The modeling processes of $CeO_2(001)$ doping into the WC/WC, WC/Co, and $CrAlSiN_{Al}$/WC-Co interfaces are shown in Figure 5a–c. The procedures for Y_2O_3 doping into the WC/WC, WC/Co, and $CrAlSiN_{Al}$/WC-Co interfaces were the same as those for CeO_2 doping.
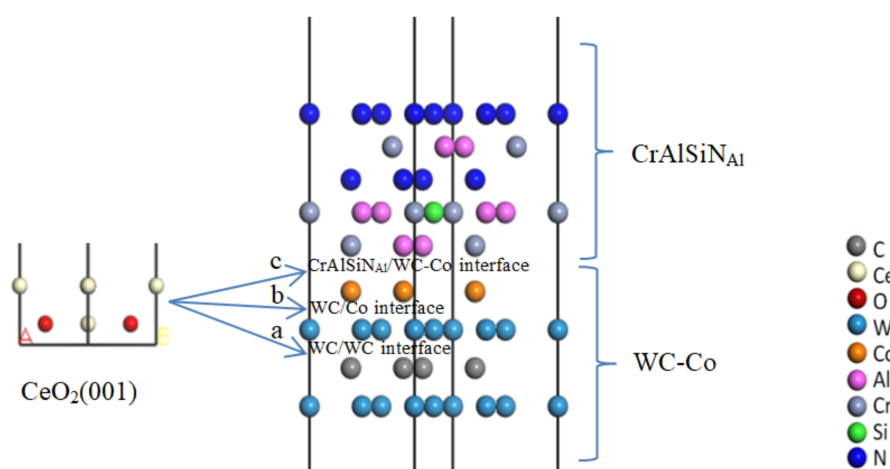

Figure 5. Construction of models doped with $CeO_2(001)$: (**a**) $CrAlSiN_{Al}$/WC/CeO_2/WC-Co model; (**b**) $CrAlSiN_{Al}$/WC/CeO_2/Co model; (**c**) $CrAlSiN_{Al}$/CeO_2/WC-Co model.

4.2. Geometric Optimization of the Doped Models

The Al terminal models doped with CeO_2 and Y_2O_3 were subjected to geometric optimization using the above parameters for simulation analysis to obtain an interface model with a stable structure. Figure 6a,b depict the optimized models with CeO_2 and Y_2O_3 doped into the WC/WC interface, respectively; Figure 6c,d present the optimized models with CeO_2 and Y_2O_3 doped into the WC/Co interface, respectively; Figure 6e,f depict the optimized models with CeO_2 and Y_2O_3 doped into the $CrAlSiN_{Al}$/WC-Co interface, respectively.

4.3. Analysis of the Interface Bonding Properties of the Al Terminal Model Doped with CeO_2 or Y_2O_3

4.3.1. Adhesion Work Analysis

The models doped with CeO_2 or Y_2O_3 all contained several interfaces. For example, in the $CrAlSiN_{Al}$/WC/CeO_2/Co model, there were three interfaces: $CrAlSiN_{Al}$/WC-Co, CeO_2/Co, and WC/CeO_2. All interface adhesion work values were calculated, as shown in Table 2, compared with the adhesion work values at the $CrAlSiN_{Al}$/WC-Co interface before doping. As long as the adhesion work value of any of the multiple interfaces included in the doping model was smaller than that of the $CrAlSiN_{Al}$/WC-Co interface before doping, CeO_2 or Y_2O_3 doping decreased the interface bonding properties of the Al terminal model. Only when the adhesion work of all interfaces in the doped model was greater than that of the $CrAlSiN_{Al}$/WC-Co interface before doping could the doping of CeO_2 or Y_2O_3 improve the interface bonding performance of the Al terminal model.
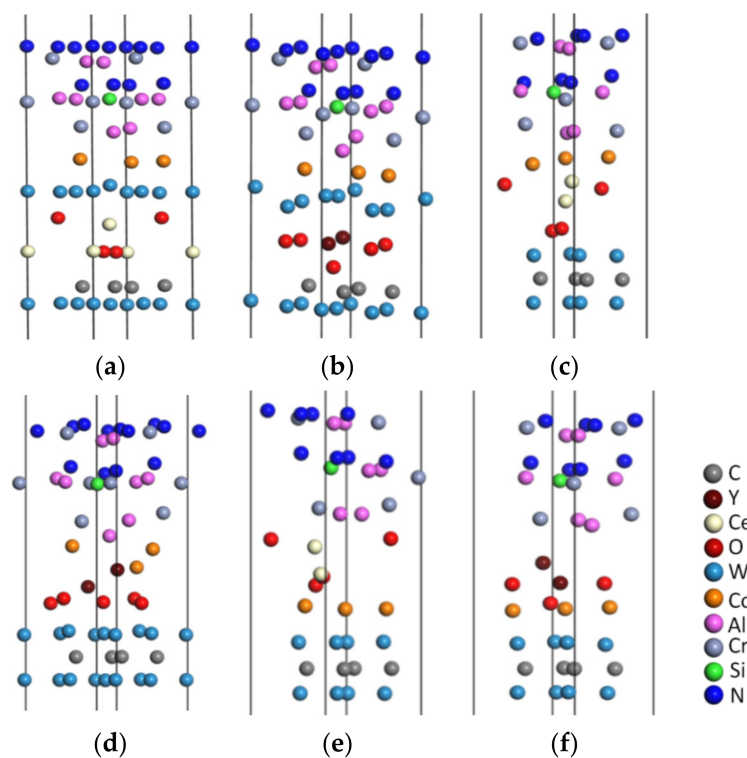
Figure 6. Doped models after geometric optimization: (**a**) $CrAlSiN_{Al}/WC/CeO_2/WC-Co$; (**b**) $CrAlSiN_{Al}/WC/Y_2O_3/WC-Co$; (**c**) $CrAlSiN_{Al}/WC/CeO_2/Co$; (**d**) $CrAlSiN_{Al}/WC/Y_2O_3/Co$; (**e**) $CrAlSiN_{Al}/CeO_2/WC-Co$; (**f**) $CrAlSiN_{Al}/Y_2O_3/WC-Co$.

Table 2. Adhesion work at different interfaces with and without CeO_2 or Y_2O_3 doping.

Doping Type	Interface Model	Interface	E_α/(eV)	E_β/(eV)	$E_{\alpha/\beta}$/(eV)	$A_{\alpha/\beta}$/(Å^2)	W_{ad}/(J·m^{-2})
Undoped	$CrAlSiN_{Al}/WC-Co$	$CrAlSiN_{Al}/WC-Co$	−14,953.219	−19,209.751	−34,167.157	26.418	2.536
Doped CeO$_2$	$CrAlSiN_{Al}/WC/$ $CeO_2/WC-Co$	$CrAlSiN_{Al}/WC-Co$ $WC-Co/CeO_2$	−14,952.436 −25,809.872	−23,075.467 −12,214.276	−38,031.572 −38,031.572	29.494 29.494	1.990 4.027
	$CrAlSiN_{Al}/WC/$ CeO_2/Co	$CrAlSiN_{Al}/WC-Co$ CeO_2/Co WC/CeO_2	−82,179.012 −78,884.118 −74,637.363	−15,042.382 −18,339.084 −22,583.294	−97,229.165 −97,229.165 −97,229.165	29.494 29.494 29.494	4.216 3.235 4.615
	$CrAlSiN_{Al}/CeO_2/$ $WC-Co$	$CrAlSiN_{Al}/CeO_2$ $CeO_2/WC-Co$	−15,041.256 −77,935.625	−82,183.017 −19,290.353	−97,229.200 −97,229.200	29.494 29.494	2.673 1.748
Doped Y$_2$O$_3$	$CrAlSiN_{Al}/WC/$ $Y_2O_3/WC-Co$	$CrAlSiN_{Al}/WC-Co$ $WC-Co/Y_2O_3$	−14,952.029 −25,808.481	−20,895.258 −10,034.951	−35,849.532 −35,849.532	30.051 30.051	1.195 3.248
	$CrAlSiN_{Al}/WC/$ Y_2O_3/Co	$CrAlSiN_{Al}/WC-Co$ Y_2O_3/Co WC/Y_2O_3	−20,905.148 −18,082.653 −16,078.979	−14,955.857 −17,778.943 −19,781.223	−35,869.075 −35,869.075 −35,869.075	30.051 30.051 30.051	4.297 3.982 4.724
	$CrAlSiN_{Al}/Y_2O_3/$ $WC-Co$	$CrAlSiN_{Al}/Y_2O_3$ $Y_2O_3/WC-Co$	−14,956.840 −19,207.037	−20,909.197 −16,652.194	−35,869.241 −35,869.241	30.051 30.051	1.706 5.330

CeO_2 was doped into the WC/WC, WC/Co, and $CrAlSiN_{Al}/WC-Co$ interfaces in the Al terminal model to obtain the $CrAlSiN_{Al}/WC/CeO_2/WC-Co$, $CrAlSiN_{Al}/WC/CeO_2/Co$, and $CrAlSiN_{Al}/CeO_2/WC-Co$ models, respectively. Y_2O_3 was doped into the WC/WC, WC/Co, and $CrAlSiN_{Al}/WC-Co$ interfaces in the Al terminal model to obtain the $CrAlSiN_{Al}/$ $WC/Y_2O_3/WC-Co$, $CrAlSiN_{Al}/WC/Y_2O_3/Co$, and $CrAlSiN_{Al}/Y_2O_3/WC-Co$ models, respectively. Table 2 shows the adhesion work calculated at different interfaces with and without doping of CeO_2 and Y_2O_3 into the WC/WC, WC/Co, and $CrAlSiN_{Al}/WC-Co$ interfaces.

It can be inferred from Table 2 that when CeO_2 and Y_2O_3 were, respectively, doped into the WC/WC interface to build two doped models, both contained the $CrAlSiN_{Al}/WC-Co$ interface, and their adhesion work values were smaller than those of the $CrAlSiN_{Al}/WC-Co$ interface before doping. That is, doping CeO_2 or Y_2O_3 into the WC/WC interface reduced the interface bonding properties of the Al terminal model.

In all doped models built by doping CeO_2 or Y_2O_3 into the WC/Co interface, the adhesion work at all interfaces was consistently higher than that at the $CrAlSiN_{Al}/WC$-Co interface before doping. In $CrAlSiN_{Al}/WC/CeO_2/Co$, the adhesion work values at the $CrAlSiN_{Al}/WC$-Co, CeO_2/Co, and WC/CeO_2 interfaces were 4.216, 3.235, and 4.615 $J\cdot m^{-2}$, respectively. In $CrAlSiN_{Al}/WC/Y_2O_3/Co$, the adhesion work values at the $CrAlSiN_{Al}/WC$-Co, Y_2O_3/Co, and WC/Y_2O_3 interfaces were 4.297, 3.982, and 4.724 $J\cdot m^{-2}$, respectively. The calculation results showed that doping CeO_2 or Y_2O_3 into the WC/Co interface enhanced the interface bonding properties of the Al terminal model.

Of the two doped models, $CrAlSiN_{Al}/CeO_2/WC$-Co and $CrAlSiN_{Al}/Y_2O_3/WC$-Co, formed by doping CeO_2 or Y_2O_3 into the $CrAlSiN_{Al}/WC$-Co interface, there were interfaces with reduced adhesion work values. In summary, doping CeO_2 or Y_2O_3 into the $CrAlSiN_{Al}/WC$-Co interface deteriorated the interface bonding properties of the Al terminal model.

In order to compare the effects of doping CeO_2 or Y_2O_3 at different interfaces of the Al terminal model on their interface bonding properties, we chose the adhesion work at the $CrAlSiN_{Al}/WC$-Co interface among the WC/WC and WC-Co interfaces doped with CeO_2 or Y_2O_3. The smallest adhesion work was chosen among the $CrAlSiN_{Al}/WC$-Co interfaces doped with CeO_2 or Y_2O_3. A comparison chart of the adhesion work was thus produced, as shown in Figure 7.
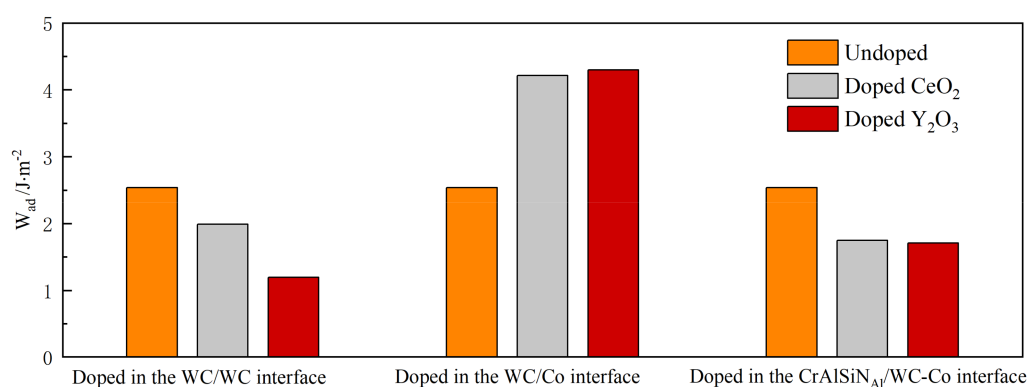

Figure 7. Comparison of the adhesion work for Al terminal model doped and not doped with CeO_2 or Y_2O_3.

As shown in Figure 7, doping CeO_2 or Y_2O_3 into the WC/WC and $CrAlSiN_{Al}/WC$-Co interfaces reduced the adhesion work compared to non-doped interfaces—that is, doping impaired the interface bonding properties of the Al terminal model. Compared with the $CrAlSiN_{Al}/WC$-Co interface adhesion work not doped with rare earth oxides, doping CeO_2 or Y_2O_3 into the WC/Co interface increased the adhesion work—that is, doping improved the interface bonding properties of the Al terminal model. After doping rare element oxides into the WC/Co interface, further analysis revealed that of the two models, $CrAlSiN_{Al}/CeO_2/WC$-Co and $CrAlSiN_{Al}/Y_2O_3/WC$-Co, the adhesion work at the $CrAlSiN_{Al}/WC$-Co interfaces was 4.216 and 4.297 $J\cdot m^{-2}$, respectively. The increase was 1.68 and 1.761 $J\cdot m^{-2}$, respectively, compared with those before doping. Compared with CeO_2 doping, Y_2O_3 doping more significantly improved the bonding properties for the Al terminal model.

4.3.2. Charge Density Difference Analysis

Geometric optimization of the doped models caused charge redistribution among the atoms. The charge density difference maps allowed for the more intuitive observation of interatomic bonding in the system. In addition, the polarity of interatomic bonds could be assessed based on the spatial distribution of charge aggregation and charge transfer. Therefore, the interface bonding properties were characterized by the bonding strength.

The charge density difference was calculated for the doped models after geometric optimization, with the results shown in Figure 8, where the regions with electron loss, gain, and zero transfer are indicated by red, blue, and white colors, respectively.
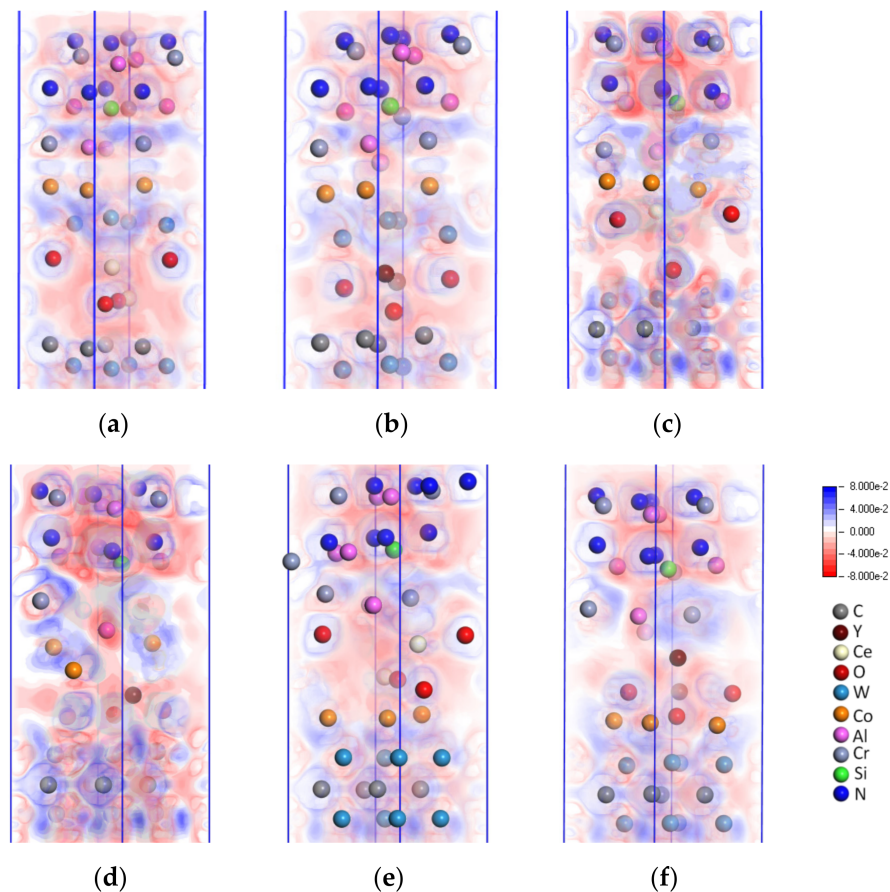

Figure 8. Charge density difference maps after doping CeO_2 or Y_2O_3 into the WC/WC, WC/Co, and $CrAlSiN_{Al}$/WC-Co interfaces: (**a**) $CrAlSiN_{Al}$/WC/CeO_2/WC-Co; (**b**) $CrAlSiN_{Al}$/WC/Y_2O_3/WC-Co; (**c**) $CrAlSiN_{Al}$/WC/CeO_2/Co; (**d**) $CrAlSiN_{Al}$/WC/Y_2O_3/Co; (**e**) $CrAlSiN_{Al}$/CeO_2/WC-Co; (**f**) $CrAlSiN_{Al}$/Y_2O_3/WC-Co.

Figure 8a,b present the charge density difference maps after doping CeO_2 or Y_2O_3 into the WC/WC interface, where regions without electrons or with low charge density existed at the $CrAlSiN_{Al}$/WC-Co interface. This result indicated that doping CeO_2 or Y_2O_3 into the WC/WC interface decreased the interatomic interactions between the $CrAlSiN_{Al}$ coating and the WC-Co matrix, thus lowering the interface bonding properties.

Figure 8c,d depict the charge density difference maps after doping CeO_2 or Y_2O_3 into the WC-Co interface. As shown in Figure 8c, the interatomic distance decreased at the $CrAlSiN_{Al}$/WC-Co interface while the superposition of charge densities was enhanced. This phenomenon was more pronounced in the blue region near the Co atom, indicating the loss of many charges. Charge aggregation was more pronounced near the Cr and Al atoms, resulting in the gain of many charges. As a result, atoms at the $CrAlSiN_{Al}$/WC-Co interface exhibited strong covalency, and the interface bonding strength increased. At the WC/CeO_2/Co interface in (c), charge transfer in Ce-W and O-Co atom pairs was significant, accompanied by increased charge density, enhanced interatomic interactions, high covalency, and high interface bonding strength. At the $CrAlSiN_{Al}$/WC-Co interface in (d), the atomic positions were changed, and charge transfer occurred between Al, Cr, and Co atoms. Interatomic interactions and covalency were strengthened, being manifested as increased bonding strength at the $CrAlSiN_{Al}$/WC-Co interface. At the WC/Y_2O_3/Co

interface in (d), the high charge density in the O-W atom pair suggested strong attraction in this atom pair and high interface bonding strength.

Figure 8e,f present the charge density difference maps after doping CeO_2 and Y_2O_3 into the $CrAlSiN_{Al}$/WC-Co interface, respectively. In the $CrAlSiN_{Al}$/CeO_2/WC-Co model, the electron clouds were superposed between Al, O, and Ce atoms, leading to strong interatomic interactions. Charge transfer occurred in the Co-O atom pair at the interface. There were shared charges between Co-O and Ce atoms, accompanied by decreased charge density and weak interatomic interactions. In the $CrAlSiN_{Al}$/Y_2O_3/WC-Co model, O and Y atoms moved away from the $CrAlSiN_{Al}$ coating. There was a greater distance between Al and O atoms, less superposition of electron clouds, and lower interatomic interactions. In contrast, the superposition of electron clouds was greater between the Co atom and O-Y, which meant stronger interatomic interactions. That is, doping CeO_2 or Y_2O_3 into the $CrAlSiN_{Al}$/WC-Co interface deteriorated the interface bonding properties of the Al terminal model. The results of the charge density difference analysis agreed with those of the adhesion work analysis.

4.3.3. Mulliken Average Bond Population Analysis

Mulliken bond population (MBP) analysis is a widely used method to calculate atomic charges. The MBP characterizes the interatomic bonding strength. A positive MBP usually indicates covalency; the higher the value, the stronger the covalency and the interatomic interactions. A negative MBP indicates antibonding, and the higher the absolute value, the more unstable the bonding, the smaller the interatomic interactions, and the greater the repulsion. Calculating the Mulliken average bond population (MABP) allows one to analyze the interatomic bonding strength better. The MABPs were calculated at the WC/WC, WC/Co, and $CrAlSiN_{Al}$/WC-Co interfaces doped with CeO_2 and Y_2O_3, as shown in Figures 9–11.
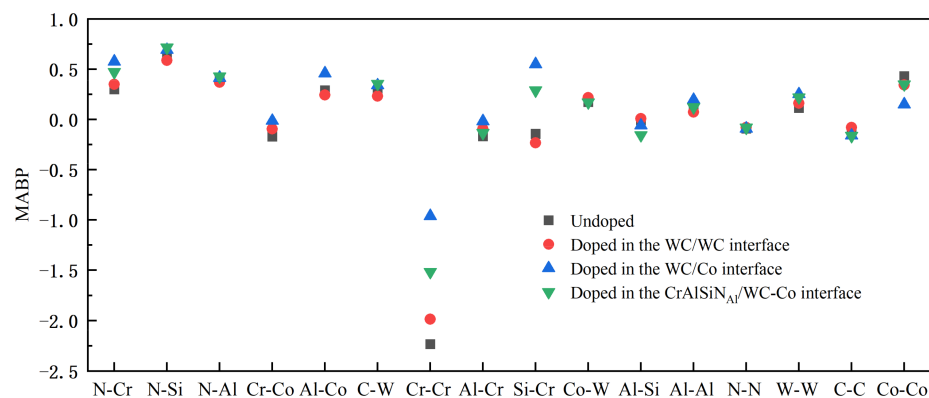

Figure 9. MABPs at different interfaces doped and not doped with CeO_2.

Figure 9 compares the MABPs between different atoms at the WC/WC, WC/Co, and $CrAlSiN_{Al}$/WC-Co interfaces doped and not doped with CeO_2. It is easy to see that when the MABP was above zero, doping CeO_2 into the WC/WC and $CrAlSiN_{Al}$/WC-Co interfaces did not dramatically increase the MABP. In addition, the MABP was generally higher if CeO_2 was doped into the WC-Co interface than if CeO_2 was not doped or doped into the WC/WC and $CrAlSiN_{Al}$/WC-Co interfaces. Increased MABP values indicated stronger covalency and higher interatomic forces. At negative MABP values, their absolute magnitudes were smallest when CeO_2 was doped into the WC/Co interface, as shown by the comparison between the four data groups. This indicated that doping CeO_2 into the WC-Co interface more significantly reduced interatomic repulsion. Compared with no doping or doping into the WC/WC and $CrAlSiN_{Al}$/WC-Co interfaces, doping CeO_2 into the WC/Co interface led to higher interatomic stability. In other words, doping CeO_2 into

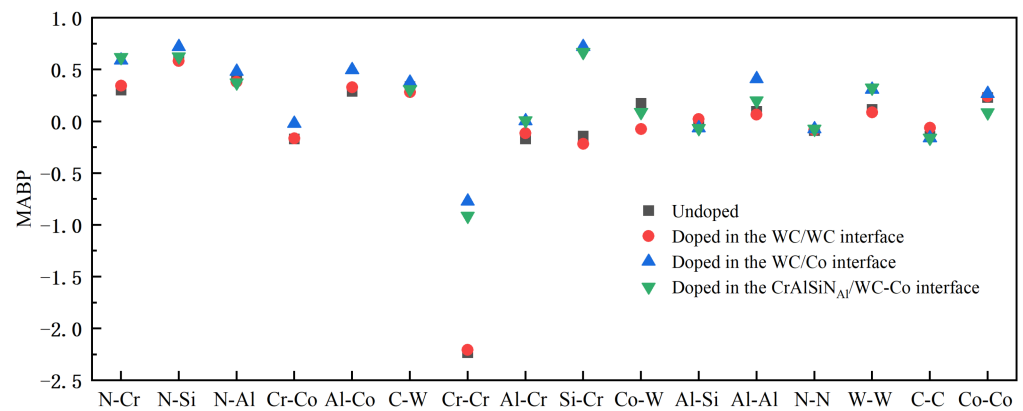the WC/Co interface improved the interface bonding strength more significantly in the Al terminal model.

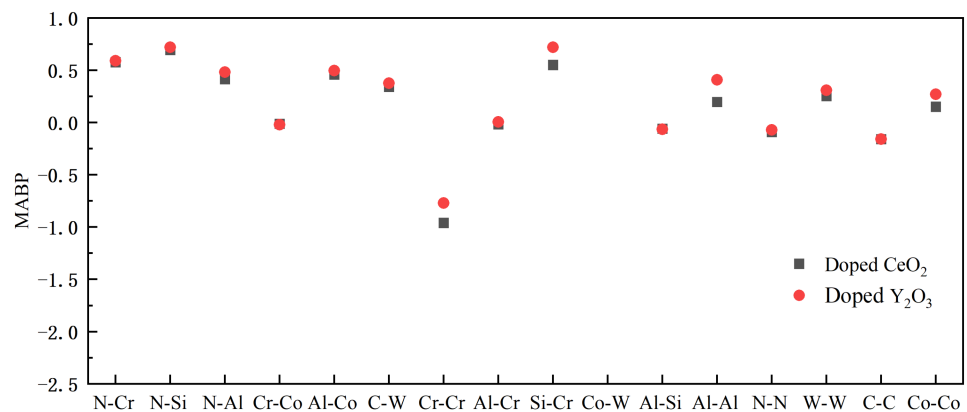**Figure 10.** MABPs at different interfaces doped and not doped with Y_2O_3.

Figure 11. Comparison of MABPs at different interfaces doped with CeO_2 or Y_2O_3.

Figure 10 compares the MABPs between different atoms after doping Y_2O_3 into the WC/WC, WC/Co, and $CrAlSiN_{Al}$/WC-Co interfaces. As shown by the figure, positive MABPs were generally higher after doping Y_2O_3 into the WC/Co interface than after not doping or doping Y_2O_3 into other interfaces. This result indicated that doping Y_2O_3 into the WC/Co interface significantly increased the interatomic forces, strengthening the interatomic bonding. When the MABPs were negative, the absolute values after doping Y_2O_3 into the WC/Co interface were generally smaller than those after not doping or doping Y_2O_3 into other interfaces. This result indicated that doping Y_2O_3 into the WC/Co interface led to higher interatomic stability than not doping or doping into other interfaces. In the meantime, the interatomic repulsion decreased, and the interface bonding properties were improved more significantly in the Al terminal model.

Figure 11 compares the MABPs after doping Y_2O_3 or CeO_2 into the WC/Co interface. When the MABP was positive, doping Y_2O_3 resulted in a higher MABP than doping CeO_2. When the MABP was negative, the absolute value after doping Y_2O_3 was smaller than that after doping CeO_2. The above results indicated that Y_2O_3 doping more significantly improved the interatomic bonding and interatomic forces than doping CeO_2. For this reason, doping Y_2O_3 into the WC/Co interface more dramatically improved the interface bonding properties of the Al terminal model.

In summary, the charge density difference analysis and MBP analysis results agreed with those of the adhesion work analysis. There is good consistency between these results and those of available experimental studies.

In particular, Wen [15] prepared a CeO_2-doped WC-10Co cemented carbide using a gas-pressure sintering furnace. The WC grain size and fracture toughness were measured

in the cemented carbides doped and not with CeO_2 using a Scanning Electron Microscope (SEM) and the press-in method, respectively. Their results showed that in the CeO_2-doped cemented carbide, the average WC grain size decreased from 530 to 410 nm after CeO_2 doping. This means that CeO_2 doping refined the WC grains. Moreover, the fracture toughness of the CeO_2-doped cemented carbide increased from 9.32 to 10.6 $MPa \cdot m^{1/2}$ after doping. The reason was that CeO_2 was enriched at the WC grain boundaries, reacting with impurity elements to purify the grain and phase boundaries. As a result, the wettability of the WC/Co interface was enhanced, as was the bonding strength of the WC/Co interface. This result agrees with our finding that doping CeO_2 into the WC/Co interface improved the bonding properties in the Al terminal model.

Wang et al. [17] prepared a Y_2O_3-doped WC-10Co cemented carbide using vacuum sintering. The cemented carbide's surface morphology and Rockwell hardness were measured by SEM and the press-in method before and after doping, respectively. The bending strength of the cemented carbides was determined using an electronic universal testing machine. The analysis revealed that Y_2O_3 doping decreased the WC grain size in the cemented carbide, thus refining the grains. Due to its high affinity, Y_2O_3 reacted with the impurities at the grain boundaries, transforming the existing form of the impurities and improving the bonding strength of the WC/Co phase. As a result, the hardness of the cemented carbide increased from HRA 92.3 before doping to HRA 94.5 after doping. The bending strength increased from 1988 MPa before doping to 2250 MPa after doping. These results agree with our finding that doping Y_2O_3 into the WC/Co interface improved the bonding properties in the Al terminal model.

Huang [18] prepared WC-10Co cemented carbides doped with Y_2O_3 and CeO_2 using a wet grid style. The surface morphology of cemented carbides before and after rare earth oxide doping was observed by SEM. The results showed that the WC grains in the cemented carbides doped with rare earth oxides were more rounded than those in non-doped cemented carbides. This was because the rounded WC grains had a larger contact area with Co, which affected the mechanical performance of the cemented carbides. The fracture toughness of the cemented carbides was determined using the Palmqvist toughness test. The fracture toughness of the Y_2O_3-doped cemented carbide (16.7 $MPa \cdot m^{1/2}$) was found to be larger than that of the CeO_2-doped cemented carbide (15.2 $MPa \cdot m^{1/2}$). In addition, the fracture toughness of Y_2O_3- or CeO_2-doped cemented carbides exceeded that of non-doped ones (12.8 $MPa \cdot m^{1/2}$). These results confirm our finding that doping Y_2O_3 into the CrAlSiN/WC-Co interface model improved the bonding properties in the Al terminal model.

5. Conclusions

(1) The adhesion work values were calculated for three interface models with various terminal atoms, namely $CrAlSiN_{Si}$/WC-Co, $CrAlSiN_N$/WC-Co, and $CrAlSiN_{Al}$/WC-Co. The analysis showed that the adhesion work was the highest at the $CrAlSiN_{Si}$/WC-Co interface (4.312 $J \cdot m^{-2}$) and the lowest at the $CrAlSiN_{Al}$/WC-Co interface (2.536 $J \cdot m^{-2}$).

(2) Based on the $CrAlSiN_{Al}$/WC-Co interface model with the lowest interface bonding strength, we doped CeO_2 or Y_2O_3 into the WC/WC, WC/Co, and $CrAlSiN_{Al}$/WC-Co interfaces to obtain the doped models.

(3) Doping CeO_2 or Y_2O_3 into the WC/WC and $CrAlSiN_{Al}$/WC-Co interfaces deteriorated the interface bonding properties of the Al terminal model; in contrast, doping into the WC/Co interface improved the bonding properties of the Al terminal model. Doping either CeO_2 or Y_2O_3 into the WC/Co interface increased the adhesion work. Further charge density difference and MABP analyses revealed that the interfaces with higher adhesion work and improved interface bonding properties exhibited a decreased interatomic distance, a higher charge density, a larger number of charge transfers between atoms, stronger interatomic interactions, a higher MABP, and higher interatomic bonding strength.

(4) Of the two rare earth oxides, Y_2O_3 doping into the WC/Co interface improved the interface bonding properties more significantly than CeO_2 doping. In $CrAlSiN_{Al}$/WC/CeO_2/Co, the adhesion work at the $CrAlSiN_{Al}$/WC-Co, CeO_2/Co, and WC/CeO_2 interfaces was 4.216, 3.235, and 4.615 J·m^{-2}, respectively. In $CrAlSiN_{Al}$/WC/Y_2O_3/Co, the adhesion work values at the $CrAlSiN_{Al}$/WC-Co, Y_2O_3/Co, and WC/Y_2O_3 interfaces were 4.297, 3.982, and 4.724 J·m^{-2}, respectively. The adhesion work with Y_2O_3 doping was consistently higher than that with CeO_2 doping. The constructed charge density difference maps revealed that Y_2O_3 doping into each interface consistently resulted in a higher charge density, a higher number of charge transfers, and stronger interatomic interactions. The MABP of the Y_2O_3-doped models was consistently higher than that of the CeO_2-doped models. These results strongly suggested that Y_2O_3 doping more significantly increased the interatomic interactions and reduced the interatomic repulsion in the Al terminal model ($CrAlSiN_{Al}$/WC-Co) compared to CeO_2 doping. Therefore, when rare earth oxides are doped at the WC/Co interface, the doping of Y_2O_3 has a better effect in terms of improving the interface bonding performance of the Al terminal model ($CrAlSiN_{Al}$/WC-Co).

Author Contributions: Conceptualization, J.Y., Y.Z. and Y.Y.; software, J.Y., Y.Y. and Y.W.; data curation, Y.Y. and Y.W.; writing—original draft preparation, J.Y., Y.Y. and Y.W.; writing—review and editing, J.Y. and Y.Y.; supervision, J.Y. and Y.Z. All authors have read and agreed to the published version of the manuscript.

Institutional Review Board Statement: Not applicable.

Informed Consent Statement: Not applicable.

Data Availability Statement: Data sharing not applicable.

Conflicts of Interest: The authors declare no conflict of interest.

Sample Availability: No samples were involved in this study.

References

1. Chang, Y.Y.; Lai, H.M. Wear behavior and cutting performance of CrAlSiN and TiAlSiN hard coatings on cemented carbide cutting tools for Ti alloys. *Surf. Coat. Technol.* **2014**, *259*, 152–158. [CrossRef]
2. Tang, Q.F.; Wang, X.; Liang, Y.M.T.; Fan, Q.X.; Wang, T.G. Study on failure mechanism of CrAlSiN-coated tool in cutting titanium alloy. *J. Tianjin Univ. Technol. Educ.* **2021**, *31*, 9–12.
3. Zhang, S.H.; Wang, L.; Wang, Q.M.; Li, M.X. A superhard CrAlSiN superlattice coatingdeposited by multi-arc ion plating: I. Microstructure and mechanical properties. *Surf. Coat. Technol.* **2013**, *214*, 160–167. [CrossRef]
4. Liu, J.; Zhu, S.S.; Xiao, X.L.; Deng, X. Study on cutting performance of dry turning Ti-6Al-4V titanium alloy with AlCrSiN coated tool. *J. Guangdong Univ. Technol.* **2021**, *38*, 99–106.
5. Hsu, C.H.; Huang, W.C.; Lee, Y.P.; Ho, W.Y. Effect of nitrogen atmosphere heat treatment on structure and wear behavior of CrAlSiN nanocomposite film. *Surf. Coat. Technol.* **2017**, *320*, 230–234. [CrossRef]
6. Lu, M.; Wang, H.; Song, X.; Sun, F. Effect of doping level on residual stress, coating-substrate adhesion and wear resistance of boron-doped diamond coated tools. *J. Manuf. Process.* **2023**, *88*, 145–156. [CrossRef]
7. Wang, Q.; Zhou, M.; Zhou, F.; Zhou, Z.; Jin, X. The toughness evaluation of CrBN coatings doped with Ni or Cu by experiment and FEM. *Appl. Surf. Sci.* **2022**, *599*, 153804. [CrossRef]
8. Yu, Y.; Mei, F.; Lin, X.; Gao, J.; Yuan, T. Impact of the B/C-doping ratio on the microstructure, mechanical properties, and cutting performance of AlTiN-based coatings. *Ceram. Int.* **2023**, *49*, 2774–2785. [CrossRef]
9. Liu, D.F. Study on Ductility-Enhancing and Strengthening Mechanism of Y Micro-Alloyed 6.5%Si High-Silicon Steel and Evolution of Microstructure and Texture in Hot and Warm Rolling. Master's Thesis, Jiangxi University of Science and Technology, Ganzhou, China, 2020.
10. Du, T. Role and mechanism of rare earth elements in metallic materials. *Trans. Nonferrous Met. Socirty China* **1996**, *6*, 15–20.
11. Li, B.; He, R.; Yang, H.; Zou, D.; Liu, Y.J.; Liang, Y.; Yang, Q.M.; Li, Y.X. Effect of Re addition on the microstructure and mechanical properties of WC-10Co cemented carbides fabricated by chemical coating method. *Int. J. Refract. Met. Hard Mater.* **2020**, *93*, 105344. [CrossRef]

12. Liu, S. Study on rare-earth doped cemented carbides in China. *Int. J. Refract. Met. Hard Mater.* **2009**, *27*, 528–534.

13. Zou, Q.; Zhang, M.L.; Li, Y.G.; Luo, Y.A. Research progress and prospect of strengtheningand toughening of WC cemented carbides. *J. Mech. Eng.* **2021**, *57*, 195–204+212.

14. Wang, Y.; Pan, Z.; Wang, C.; Sun, X.; Peng, Z.; Wang, B. Cutting performance of WC-Co alloys modified by nano-additives. *J. Mater. Sci. Technol.* **2012**, *28*, 205–213. [CrossRef]

15. Wen, Y. Effect of Rare Earth and Copper on Microstructure and Properties of WC-10Cocemented Carbide. Master's Thesis, Jiangxi University of Science and Technology, Ganzhou, China, 2019.

16. Guo, S.D.; Bao, R.; Yang, J.G.; Chen, H.; Yi, J.H. Effect of Mo and Y_2O_3 additions on the microstructure and properties of fine WC-Co cemented carbides fabricated by spark plasma sintering. *Int. J. Refract. Met. Hard Mater.* **2017**, *69*, 1–10. [CrossRef]

17. Wang, H.L.; Wang, L.S. Effect of Y_2O_3 on properties of WC-10CO cemented carbides. *China Tungsten Ind.* **2020**, *35*, 63–67.

18. Hang, C.G. Effects of rare earth Y, Ce and their addition methods on microstructure and properties of cemented carbides. *Mater. Sci. Eng. Powder Metall.* **2014**, *19*, 701–706.

19. Yang, Y.; Luo, L.M.; Zan, X.; Zhu, X.Y.; Zhu, L.; Wu, Y.C. Synthesis of Y_2O_3-doped WC-Co powders by wet chemical method and its effect on the properties of WC-Co cemented carbide alloy. *Int. J. Refract. Met. Hard Mater.* **2020**, *92*, 105324. [CrossRef]

20. Qin, Y.Q.; Peng, Y.Q.; Tian, Y.; Luo, L.M.; Ma, Y.; Zan, X.; Zhu, X.Y.; Wu, Y.C. Effect of Y_2O_3 on microstructure and mechanical properties of WC-Co-cemented carbides prepared via solid-liquid doping method and spark plasma sintering. *Mater. Today Commun.* **2020**, *24*, 101096. [CrossRef]

21. Deng, X.C.; Wang, K.F.; Zhang, G.H. Effects of oxide addition on structure and properties of WC–10Co cemented carbide obtained by in situ synthesized powder. *Int. J. Appl. Ceram. Technol.* **2022**, *19*, 1916–1928. [CrossRef]

22. Yang, J.R.; Tang, M.H.; Li, S.L.; Xu, X.Z. First-principles study of WC-Co (0001)/cBN (111) interface bonding properties. *J. Synth. Cryst.* **2020**, *49*, 485–493.

23. Wang, C.; Wang, C.Y. Ni/Ni3Al interface: A density functional theory study. *Appl. Surf. Sci.* **2009**, *255*, 3669–3675. [CrossRef]

24. Li, Y.F.; Gao, Y.M.; Xiao, B.; Min, T.; Fan, Z.J.; Ma, S.Q.; Yi, D.W. Theoretical study on the electronic properties and stabilities of low-index surfaces of WC polymorphs. *Comput. Mater. Sci.* **2011**, *50*, 939–948. [CrossRef]

25. Christensen, M.; Wahnström, G. Effects of cobalt intergranular segregation on interface energetics in WC-Co. *Acta Mater.* **2004**, *52*, 2199–2207. [CrossRef]

26. Zhang, S.H.; Wang, L.; Wang, Q.M.; Li, M.X. A superhard CrAlSiN superlattice coating deposited by a multi-arc ion plating: II. Thermal stability and oxidation resistance. *Surf. Coat. Technol.* **2013**, *214*, 153–159. [CrossRef]

27. Haršáni, M.; Sahul, M.; Zacková, P.; Čaplovič, L. Study of cathode current effect on the properties of CrAlSiN coatings prepared by LARC. *Vacuum* **2017**, *139*, 1–8. [CrossRef]

28. Zhang, G.A. Preparation and Mechanical Properties of CrN Composite Films and Al-DLC Films. Master's Thesis, Lanzhou University, Lanzhou, China, 2008.

29. Liu, C.B.; Wang, P.; Huang, F.; Li, C. Improved mechanical and thermal properties of CrAlN coatings by Si solid solution. *Vacuum* **2016**, *125*, 180–184. [CrossRef]

30. Liang YM, T.; Fan, Q.X.; Wang, X.; Wang, T.G.; Liu, Y.M.; Cao, F.T. Microstructure and properties of CrAlN nano-gradient coatings. *Surf. Technol.* **2021**, *50*, 348–355.

31. Hang, Z.Q. Study on High Temperature Resistance and Interface First-principles Calculation of RareEarth Modified WC-Co Coatings. Master's Thesis, Southwest Jiaotong University, Chengdu, China, 2018.